

Experimental Study and Finite Element Analysis of Racking Resistance subjected to varied mortise-tenon joints and wedge configurations

J.Z. CHEN¹, M INAYAMA², K AOKI³

ABSTRACT: The column–Nuki frame, a key structural system in traditional timber architecture, is primarily assembled using mortise-tenon joints and secured with wedges, significantly enhancing its seismic performance. To gain a deeper understanding of the racking resistance of column–Nuki joints with different mortise–tenon configurations and wedge placements, a series of cross-shaped specimens were constructed and subjected to lateral reciprocating static tests. In this study, 3D nonlinear finite element models were developed for each specimen to assess the applicability of numerical simulations in evaluating the seismic performance of various column–Nuki joints. The FE models were validated by comparing simulation and experimental results, including initial stiffness, load-bearing capacity, and overall deformation behavior. The comparison confirmed that the FE analysis provides an accurate prediction of racking resistance, offering a reliable approach to evaluating and optimizing traditional timber joints for improved seismic performance. The findings contribute to a better understanding of structural behavior in traditional timber construction and provide quantitative insights for future studies on timber seismic engineering, heritage conservation, and modern applications of traditional wood joinery.

KEYWORDS: Column–Nuki joint, Mortise–tenon, Wedge, Finite element, Racking resistance

1 – INTRODUCTION

China has a long history of timber architecture, with two primary construction methods for official and dwelling structures: post-and-lintel and Chuan-Dou construction. The latter remains prevalent in rural Southwest China. Chuan-Dou structures share similarities with Japanese timber structures, employing mortise–tenon joints without metallic fasteners. Columns interlock with multiple lateral members known as “Fang” in Chinese and “Nuki” in Japanese, using joints reinforced by plugs or wedges. This method ensures structural stability, economic efficiency, and superior seismic resistance, relying on embedment and frictional resistance at column–Nuki joints[1,2,3]. The tightness of wedges, determined by their initial insertion and fixation, significantly affects joint rigidity. While timber joints exhibit low rotational resistance, their ductile embedment behavior contributes to high deformability, enhancing seismic performance.

However, severe earthquakes can induce excessive deformation and damage, particularly at column–Nuki joints, leading to potential structural instability. Field investigations in Southwest China have identified pulling-out failures, shear cracks, and splits as primary failure

modes of mortise–tenon joints[4,5]. Since traditional Chuan-Dou structures rely on empirical construction methods with limited supervision, ensuring consistent quality remains challenging. Consequently, research on deformability and bearing capacity evaluation has gained increasing attention. Experimental studies on mortise–tenon joint configurations, including wood species, joint dimensions, and wedge arrangements, are essential. Given that column–Nuki frames provide lateral resistance against earthquakes, numerous studies have explored their seismic performance. However, preparing full-scale specimens is time-consuming and labor-intensive, limiting experimental feasibility. Therefore, researchers have increasingly adopted mechanical modeling, formulations, and finite element analysis(FEA) to improve the understanding of seismic resistance mechanisms[6,7,8].

2 – BACKGROUND

FEA has proven valuable in simulating rotational embedment behaviors, particularly in evaluating moment resistance and racking performance. Despite advances in moment resistance modeling for traditional timber joints in Japan, experimental and formulaic approaches struggle

¹ Jiuzhang CHEN, Graduate School of Agricultural and Life Sciences, University of Tokyo, Tokyo, Japan, chen-jiuzhang@g.ecc.u-tokyo.ac.jp

² Masahiro INAYAMA, Holzstr Architects Co Ltd, Tokyo, Japan, tp9c-inym@asahi-net.or.jp

³ Kenji AOKI, Graduate School of Agricultural and Life Sciences, University of Tokyo, Tokyo, Japan, aoken@g.ecc.u-tokyo.ac.jp

to capture contact deformations between wedges, columns, and Nuki. Nonlinear 3D FEA has emerged as a promising alternative, offering detailed insights into stress and strain distributions. By validating numerical models against experimental results, researchers can conduct parametric studies on various joint configurations to optimize seismic performance. Recent studies have applied general-purpose FEA software such as ANSYS or ABAQUS to traditional timber structures. Liu et al.[9] modeled column-foot joints with through-tenons and dovetail-tenons under cyclic loading. Chang et al. [10] analyzed mortise-tenon joints in Taiwanese timber structures, examining the impact of wood properties on joint stiffness. Luo et al.[11] compared experimental and numerical stiffness matrices for semi-rigid joints, while Chen et al.[12] developed a VUMAT subroutine for ABAQUS to model wood behavior accurately. Guan et al.[13] simulated wedge insertion processes, validating initial stress distributions against experimental results. Additionally, Aloisio et al.[14] proposed an empirical hysteresis modeling approach using MATLAB and Python for timber joints.

Most previous studies have focused on regular through-tenon joints, lacking comprehensive analyses of alternative mortise-tenon configurations. To address this gap, this study investigates three representative column-Nuki joint types, which are through joint, Ryakukama joint, and half-lap joint with a plug—selected from field surveys in Southwest China and Japan. Additionally, three wedge configurations with varying insertion angles and tightness are examined for their effects on initial stress states. A lateral pseudo-static test is conducted to assess the bearing capacity and rigidity of timber frames with different mortise-tenon joints. A 3D nonlinear FE model is developed to simulate wedge insertion, joint deformation, damage, and racking performance. Numerical results are compared with experimental findings to validate the FE model and evaluate moment resistance across joint types and wedge configurations.

This study provides new insights into traditional mortise-tenon joints, offering a validated FE modeling approach for numerical simulations. By refining seismic performance evaluations of Chuan-Dou timber structures, this research contributes to improving the resilience and preservation of traditional timber architecture.

3 – PROJECT DESCRIPTION

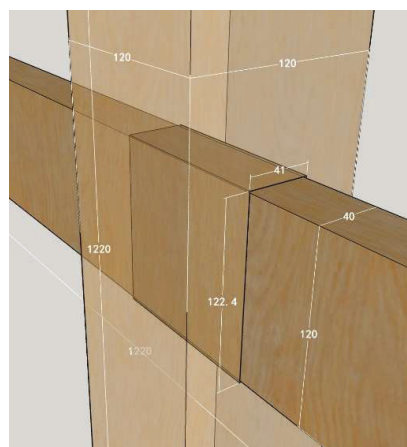
The test specimen was assembled using an E90 graded Japanese cypress (*Chamaecyparis obtuse*, with an average moisture content of 12.5% and density of 497 kg/m³) column as a vertical component (with a cross-section of 120 mm × 120 mm and length of 1200 mm) and Japanese cypress “Nuki” as lateral component (with a cross-section of 40 mm × 120 mm and length of 1200 mm). Six types of traditional column-Nuki joints with typical sizes were designed and fabricated in this study and are shown in Fig.

1. Three of these were specimens with different mortise-tenon joints, including the through joint, Ryakukama joint, and half-lap joint with a plug. As the through joint (designated as TJ) was composed of a single Nuki component without any form of connection in the contact areas of the joint, it was considered the initial prototype specimen. For the Ryakukama joint (designated as RK), the cheek of each Nuki member was designed to be overlapped and connected vertically instead of the general horizontal overlapping considered in previous research. Half-lap joint (HL) members were overlapped vertically as well. They were then fixed to the column using a square wooden plug (with a cross-section of 24 mm × 24 mm and a length of 200 mm) in the middle of the joint. The other three specimens are based on regular through joints with different wedge configurations, which are related to various factors that may have an effect on initial stress and share an identical width of Nuki (40 mm). The details of the insertion angle, tightness, and dimensions of each wedge configuration adopted in this study are listed in Table 1.

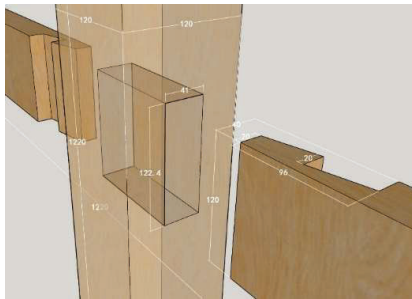
Table 1. Wedge configurations of embedding test

Specimen	Embedding height (mm)		Embedding length (mm)	Tightness (mm)	Insertion angle
	top	bottom			
TJ3-Δ1	19.5	14	60	1	10°
TJ3-Δ1.5	9	4	60	1.5	0°
TJ3-Δ2	24	18	60	2	15°

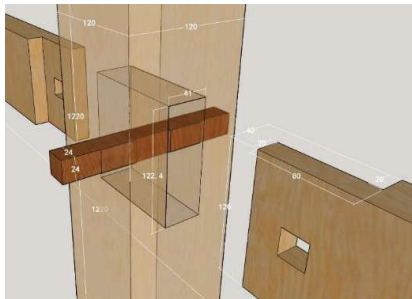
The flat-shaped wedge is primarily inserted into the lower clearance between the column opening and Nuki with a tightness of 0 mm oversizing. The left- and right-side wedges are then inserted and knocked into the upper clearance using a wooden hammer to reach the predetermined tightness. The square wooden plugs and wedges were made of Japanese evergreen oak (*Quercus acuta*, with an average moisture content of 10.9% and density of 795 kg/m³).



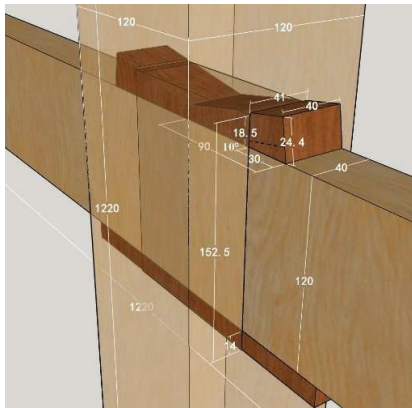
(a) Through joint (TJ)



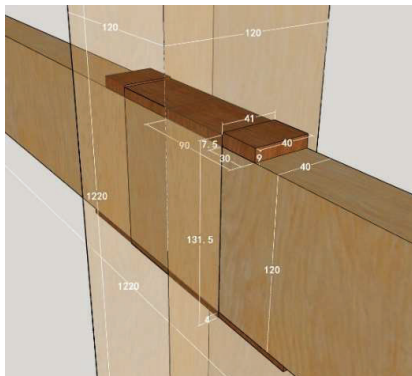
(b) Ryakukama joint (RK)



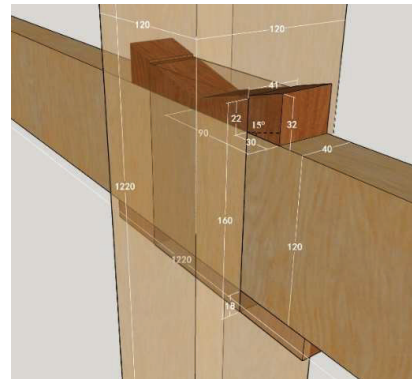
(c) Half-lap joint with a plug (HL)



(d) Through joint with wedges-TJ3-Δ1



(e) Through joint with wedges-TJ3-Δ1.5



(f) Through joint with wedges-TJ3-Δ2

Figure 1. Specifications of column–Nuki joint specimens (unit: mm)

4 – EXPERIMENTAL SETUP

The lateral reciprocating static test setup for the column–Nuki joint specimens is shown in Fig. 2. The cross-shaped specimen in the middle was secured by the surrounding wooden frame members connected by oversized straight joints, ensuring that the target specimen moved only along the lateral loading direction to eliminate out-of-plane instability to the maximum extent. The test specimens and frame members were fixed and fastened using M26 wooden rods such that they could be considered pin connections. Screws with a length of 110 mm were driven into both sides of each mortise opening along the longitudinal direction to prevent the splitting that might occur around these joints during the loading process.

The adopted testing method refers to the displacement control loading system recommended by “the Japanese allowable stress calculation for houses constructed using the wooden framework method” [15]. The load cell was set to apply a cyclic load 1000 mm from the upper loading point of the column to simulate the lateral load, which was exerted on a graded basis via a rotational angle based on displacement control. The load was exerted three times for each loading circle with an increment of rotational angle (1/200, 1/150, 1/100, 1/75, 1/50, 1/30, 1/20, and 1/10 rad) before reaching its maximum range $\pm 1/7$ rad owing to the restriction of the wooden frame. The test was terminated when the maximum rotational angle was reached or when the specimen was observed to undergo fatal damage as the load dropped significantly.

The rotational angle of the joint center was defined as the ratio of the sum of the relative displacements on both the upper and lower sides of the joint divided by the distance between the two displacement transducers located on the left and right sides of the joint.

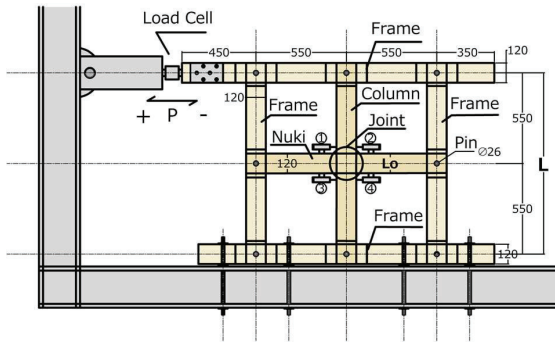


Figure 2. Test set-up for a column–Nuki joint. (unit: mm)

The rotational moment in the joint center could be obtained by multiplying the applied lateral load by the distance from the loading point to the supporting point of the column with the length of the opening for Nuki removed. The rotation angle and rotational moment are given by

$$\theta = \frac{\left(\frac{d(2)-d(1)}{2}\right) + \left(\frac{d(3)-d(4)}{2}\right)}{\Delta|1-3|} \quad (1)$$

$$M = P \times (L - L_0) \quad (2)$$

P : lateral load (N), L : distance from the loading end to the fixed end, L_0 : height of Nuki, M : racking moment (N*mm).

5 – EXPERIMENTAL RESULTS

In the case of the through joint shown in Fig. 3(a), the deformation due to the embedment of the Nuki and mortise opening was visibly confirmed when the rotation angle reached 1/30 rad. The tests concluded at a rotation angle of 1/6 rad, at which point no damage or failure other than embedment was observed at the Nuki. Fig. 3 (b) and Fig. 3 (c) show the typical failures of the Ryakukama and plug-reinforced half-lap joints at a rotation angle of 1/7 rad, respectively. From a rotation angle of 1/20 rad onward, distinct sounds of wood rupture were heard, accompanied by a tendency for the opposite end of the joint to be pulled in the reverse direction during loading. At a rotation angle of 1/10 rad, a loud fracturing sound was observed, which was attributed to the shearing failure of the tenon's interlocking jaw of the Ryakukama joint and the square hole of the half-lap joint. The Ryakukama joint experienced complete shear failure at the tenon jaw originating from the corners of its interlocking edge. Cracks and fractures induced by bending of the tenon head and propagating along the longitudinal direction could also be observed, some of which extended to the side surfaces of the Nuki. In the half-lap joint, splitting initiated from the two corners of the square plughole along the loading direction and extended to the outermost edges, causing severe shearing damage.

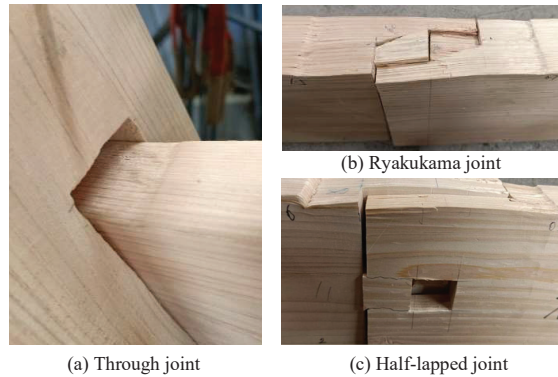


Figure 3. Embedment and shear failure of column–Nuki joints

The moment resistance characteristic values for a typical wooden frame, such as M_y is obtained by parallel-shifting the line connecting 0.4 M_{max} and 0.9 M_{max} until it tangentially touches the curve as shown in Fig. 4. The corresponding rotation angle at this point is θ_y . K_I is the slope of the line connecting the points $(\theta_0, 0)$ and (θ_y, M_y) , where θ_0 is the rotation angle corresponding to the intersection of the extended line (from 0.1 M_{max} to 0.4 M_{max}) with the X-axis.

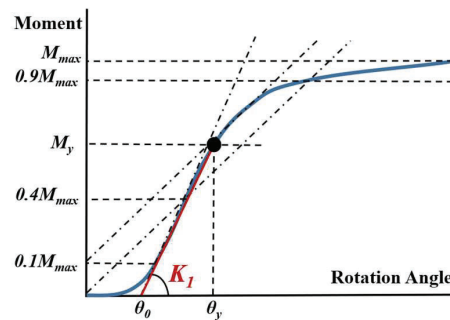


Figure 4. Moment resistance characteristic values

A theoretical evaluation method based on the rotational embedment model of a through joint proposed by Sauda [16], shown in Fig. 5, was derived to obtain the initial stiffness K_θ and the yield point (θ_y, M_y) . In these equations, the strain energy is assumed to be constant at the yielding stage and the clearance factor is considered.

The initial stiffness is closely related to the full-area compressive Young's modulus perpendicular to the grain, E_{90} . In this study, the corresponding Young's modulus of the Nuki with wood species of Japanese cypress applied for the theoretical evaluation was determined from “the Japanese design manual for engineered timber joints” [17] as $E_{90_cypress} = E_{0_cypress} / 50 = 180 \text{ N/mm}^2$. However, for joints with wedges made of hardwood such as Japanese evergreen oak, as the surface of hardwood is considered to be much harder than that of Nuki made of softwood, the compressive Young's modulus perpendicular to the grain E_{90} of the wedges was set as $E_{90_evergreen\ oak} = E_{0_evergreen\ oak} / 50 = 280 \text{ N/mm}^2$ to restore the fastening effect of wedges and improve the evaluation accuracy of initial stiffness in cases of joints with wedges.

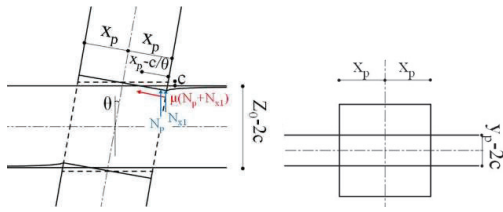


Figure 5. Rotational embedment model of a through joint considering the clearance

$$C_{xm} = 1 + \frac{2}{ax_p}, C_{ym} = 1 + \frac{2}{any_p} \quad (3)$$

$$\theta_y = \frac{\sqrt{C_{ym}\{2ax_p F_m^2(ax_p + 2)(z_0 - 2c)^2 + C_{xm}C_{ym}E_{90}^2c^2\}}}{\{\sqrt{C_{xm}C_{ym}E_{90}x_p(ax_p + 2)}\} + \frac{\sqrt{C_{xm}C_{ym}E_{90}c(ax_p + 1)}}{\{\sqrt{C_{xm}C_{ym}E_{90}x_p(ax_p + 2)}\}}} \quad (4)$$

$$K_\theta = \left(x_p - \frac{c}{\theta_y}\right)(y_p - 2c)E_{90} \times$$

$$\left[\frac{2}{z_0 - 2c} \left\{ \frac{\left(x_p - \frac{c}{\theta_y}\right)\left(2x_p + \frac{c}{\theta_y}\right)}{6} + \frac{x_p}{a} \right\} + \mu \left\{ \frac{\left(x_p - \frac{c}{\theta_y}\right)}{2} + \frac{1}{a} \right\} \right] \quad (5)$$

x_p : half the face width of the column (mm), y_p : depth width of the “Nuki” opening (mm), z_0 : face width of the “Nuki” opening (mm), c : half the initial clearance (mm), E_{90} : young’s modulus of compression perpendicular to the grain, assuming $E_{90} = E_0/50$ (N/mm²), F_{cv} : standard partial compression strength in the middle section of “Nuki” (N/mm²), F_m : embedding yield stress when the edge distance is considered infinite, assuming that $0.8F_{cv} = F_m$ (N/mm²), N_p : reaction force right under the rotational embedment (N), N_{xl} : reaction force due to the excess length in the x-direction of the rotational embedment (N), n : substitution coefficient for the direction perpendicular to the grain, a : coefficient determining the extent of deformation of the excess length portion, assuming $a = 5.5/(z_0 - 2c)$, μ : friction coefficient considering embedment of joint members, assuming 0.6 for through joints, 0.4 for Ryakukama joints, and 0.5 for half-lap joints.

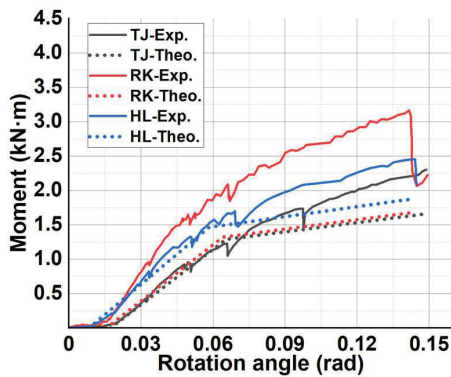
The typical skeleton curves of the moment–rotation relationship and the results derived from the theoretical formulas of typical specimens for each specified joint type are shown in Fig. 6, where subfigures (a) and (b) show comparisons of joints with different mortise–tenon types, including through, Ryakukama, and half-lap joints, as well as other with varied wedge configurations. The characteristic values obtained from both the experiments and theoretical evaluations are listed in Table 2. From the results, the bearing capacity of mortise–tenon joints without wedges increased slowly in the early stage owing to the existence of vertical clearance between the mortise opening and the Nuki. Meanwhile, the prototype specimen

TJ with a through joint showed the overall lowest rigidity and bearing capacity compared with those of the other two forms of mortise–tenon joints. The Ryakukama joint showed an unexpectedly high rigidity that could be rarely found in pure mortise–tenon joints without any reinforcement, and it is speculated that the friction between the side areas of the mortise opening and tenon cheeks might contribute significantly to this behavior as the specimen consistently moved in the lateral direction. Even though the lateral clearance for each side of the joint was originally set as 0.5 mm, a certain amount of manual errors can appear when fabricating and assembling the specimens, which could be hard to eliminate in an actual construction process. The initial rigidity of a typical half-lap joint can be properly predicted by the previously described theoretical evaluation method. The form of the mortise–tenon joint seems to play a relatively irrelevant role in the early plastic stage, and it cannot be precisely described by the commonly used formula for general timber joints.

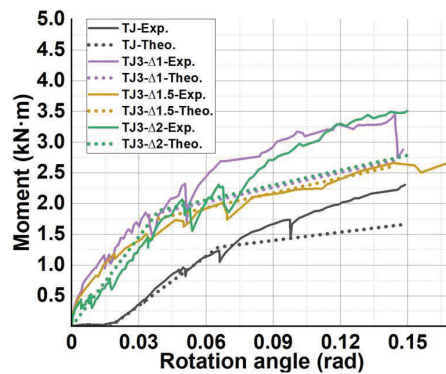
It was observed in a series of experiments that the rigidity of joints with wedges was significantly higher than that of through and mortise–tenon joints. In joints reinforced with wedges, the initial stiffness values remained nearly constant at approximately 48.5–48.7 kN·m/rad across all wedge configurations, but they failed to predict the particular wedge configuration of a certain joint specimen. The wedge configurations and insertion conditions could significantly influence the initial stiffness. Thus, the current theoretical formulas for through joints must be further modified to properly describe the early-stage rigidity performance of joints with different wedge configurations. This highlights the limitation and imprecision of the prevailing theoretical evaluation methods in Japan for various traditional joints, especially joints with non-uniform wedge configurations.

Table 2. Characteristic values of moment resistance

Specimen	θ_y	M_y	$K_{Exp.}$	$K_{Theo.}$	$K_{Theo./K_{Exp.}}$
	rad	kN·m	kN·m/rad	kN·m/rad	
TJ	0.046	0.89	32.8	26.8	0.82
RK	0.045	1.54	47.2	27.2	0.58
HL	0.047	1.29	32.3	30.1	0.93
TJ3-Δ1	0.041	1.88	65.3	48.7	0.75
TJ3-Δ1.5	0.048	1.72	62.7	48.5	0.77
TJ3-Δ2	0.059	2.26	34.9	48.6	1.39



(a) Comparison with mortise-tenon joints



(b) Comparison with wedge-reinforced through joints

Figure 6. Comparison of the relationship between rotation angle and moment

6 –FINITE ELEMENT ANALYSIS

6.1 MODELING

In this study, numerical modeling and simulation of the racking performance of typical types of column–Nuki joints were conducted using the general FEA software ABAQUS, and the Explicit solver was adopted to improve the prediction accuracy and efficiency in large deformation and sliding friction situations. Wood, as the dominant material in the simulation, was simplified as an orthogonal anisotropic material for the numerical simulations. Two species of wood were used for the joint model: Japanese cypress (softwood) for the column and Nuki and Japanese evergreen oak (hardwood) for wedges and plugs. The wooden joint was primarily considered as an elastic-perfect plastic model at the early loading stage, with small displacements and elastic deformation. After entering the yield stage, local high-stress concentration and significant plastic deformation were likely to occur on embedment regions of the Nuki, with an enlargement of racking displacements. Therefore, the elastoplasticity of the joint model was modified by adding the strain hardening law to better illustrate the hardening behaviors of the Nuki in the crucial contact areas induced by localized embedment. The elastic properties of each wood material were described using nine engineering constants, among which the

Young's modulus data in three orthotropic directions (longitudinal, radial, and tangential), listed in Table 3, were obtained from previously conducted full compressive tests of small clear specimens. The other plastic stage constants (shear modulus and Poisson's ratio) were obtained from previous studies on the orthotropic properties of wood. As for the plastic stage, the initial yield stress and stress hardening law of the Nuki were used together with the potential function in Abaqus defined by Hill's yield criterion, and are listed in Table 4. In this study, the stress hardening law was interpreted as the hardening stress and corresponding plastic strain, namely, true stress (σ) and true strain (ε), which were derived from the experimental stress and strain results of the aforementioned full compressive tests perpendicular to the grain.

Table 3. Wood properties of FEA

		Japanese cypress		Evergreen oak		
Young's modulus /MPa	E_L	13118	16100	R_{11}	7.35	1.95
	E_R	1063	1948	R_{22}	1	1
	E_T	604	1063	Initial yield stress ratio R_{33}	1	1
Shear modulus /MPa	G_{LR}	958	1481	R_{12}	1.94	2.12
	G_{LT}	603	1014	R_{13}	1.34	1.51
	G_{RT}	40	386	R_{23}	0.23	1.56
Poisson's ratio	ν_{12}	0.4	0.41			
	ν_{13}	0.62	0.52			
	ν_{23}	0.53	0.67			

Table 4. Yield stage specification

Japanese cypress in tangential direction		Japanese evergreen oak in radial direction	
Yield Stress	Plastic Strain	Yield Stress	Plastic Strain
2.79627	0.00000	24.63	0
2.85374	0.00016	45.49	0.121
2.91122	0.00032		
2.96619	0.00047		
3.01617	0.00062		
3.06115	0.00076		
3.10114	0.00090		
.....		
3.83581	0.00506		
3.83581	0.00509		
3.84081	0.00512		
3.84081	0.00514		
3.84331	0.00518		
3.84331	0.00520		
3.84581	0.00523		

A typical column–Nuki model (with wedges in this case) and its simplified boundary conditions are illustrated in Fig. 7 with the longitudinal, tangential (vertical), and radial (out-of-plane) directions of the Nuki as the 1-, 2-, and 3-axis, respectively. An eight-joint hexahedral linear unit C3D8R was used for the meshing. The mesh size of the wedges was 5 mm and that of the column and Nuki in crucial contact regions was set to 8 mm, whereas the mesh sizes of the other regions were set from 15 to 30 mm in a gradually increasing pattern based on their dimensional proximity to the crucial interface regions. To reduce stress concentration at the edges of the model, which were identified as the load and restraint ends, reference points were set and coupled at coordinates 50 mm away from the column head and 5 mm away from both ends of the Nuki in the lateral loading direction known as 1-axis. Another reference point for the boundary conditions was the pinhole of the column base. For joint models without wedges, only one loading step was used to complete the loading simulation. The loading process was carried out by customized incremental rate control in the lateral direction applied to the reference points located at the column head and both ends of the Nuki model, and possible displacement and rotation in the other two directions (2-axis, 3-axis) were strictly set to zero to eliminate the possibility of inducing out-of-plane displacement. Meanwhile, the column was only considered to pass through certain rotation angles around the 3-axis with the column base as the reference point. When the rotation angle at the reference point of the column base, which was converted from the ratio of lateral displacement to length of the column, reached approximately 0.2 rad, the simulation was considered complete. For joint members with wedges, there was an additional insertion step immediately before the loading step to investigate the initial stress state of the inserted wedges, which was later validated by the experimental results of the embedding test for wedges. The step time for both the insertion and loading steps was set to 0.1. During the insertion step, wedges on both sides of the column were simultaneously introduced into the column opening, with the predefined embedding length of the wedges set to 60 mm, corresponding to half of the column width of the experimental dimensions. The column–Nuki joint model was fully constrained to avoid any possible instability during the insertion step, and the wedges were only controlled by displacement in the lateral direction and were fully constrained in the other two directions. For the loading step, the constraints in the vertical direction on the wedges were released to simulate their possible slip behavior during the loading process. The friction coefficients of the interfaces of the joint members were set to 0.3 for the through joint, 0.2 for the Ryakukama joint, and 0.25 for the half-lap joint.

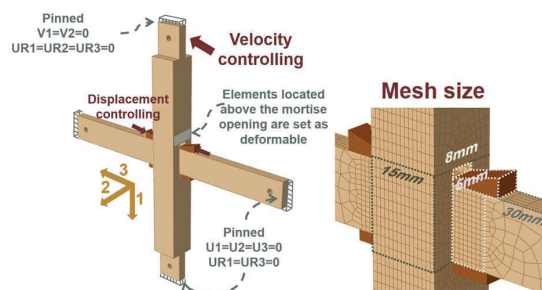


Figure 7. Boundary conditions and meshing of a column–Nuki joint model

6.2 COMPARISON WITH EXPERIMENTAL RESULTS

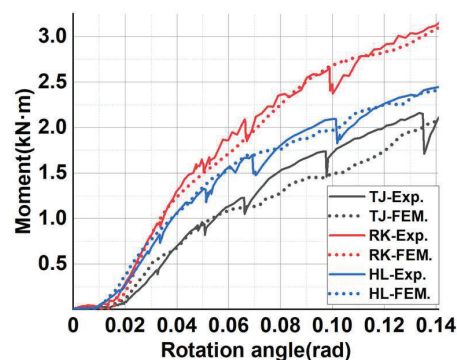
Fig.8 compares the moment–rotation relationship in skeleton curves of experimental results and FEA results among three types of mortise–tenon joint forms, including a through, Ryakukama, and half-lap joint, together with a through joint in combination with inserted wedges under three different wedge configurations considering variations in wedge dimension and tightness. A comparison of the initial stiffness between the experimental and FEA results obtained when the rotation angle reached 0.14 rad is presented in Table 5. The moment–rotation relationship of the through and mortise–tenon joints had a reasonably good correlation with experimental results. For a through joint, the FEA result for the initial stiffness was approximately 1.03 times the experimental result, which is in good agreement with the experimental results. Both the initial stiffness and yield moment of the Ryakukama and half-lap joints obtained from the FEA were in close agreement with the experimental results; only the tertiary stiffness appeared to be slightly lower than the experimental result. A possible reason for the trivial deviation is that the constitutive model of the wood material adopted in this study did not include any form of damage model. Thus, possible experimental damage, such as small splitting or cracks induced by shear force and tension in the crucial contact areas within the engaged joint, could not be ideally evaluated by the current finite element model. These interface areas, particularly on the edges and corners of the engaging part of a tenon, tend to have a high stress concentration that already exceeds the ultimate shear strength, which could lead to splitting or shear damage. The insufficiency of the constitutive model of wood resulted in the inability to predict the occurrence and evolution of damage in crucial contact areas and significantly simplified the cumulative embedding, squeezing, and concomitant friction development when the aforementioned local damage occurred under realistic loading conditions. The details of the stress distribution and deformation for each type of mortise–tenon joint are further discussed in the following subsection.

For through joints with different wedge configurations, a comparison of the moment–rotation angle relationship revealed that the overall trend of increasing moment in the elastic stage of the FEA results closely matched the

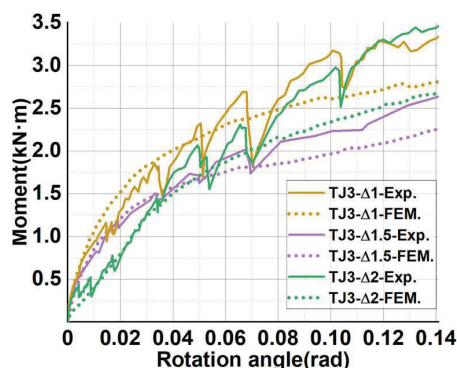
experimental results, indicating that the wedge insertion process and, consequently, the initial stress could be successfully simulated using the finite element method, and the racking resistance performance of the joints during the elastic stage could be predicted as well. The FEA results showed a clearer yield point than the experimental results, and the moment–rotation angle relationships were more inclined to display distinct double linear features characterized by a yield point and mild secondary stiffness, presenting distinct post-yield hardening behaviors. Comparing the characteristic values, the initial stiffness of the FEA result for the joint with wedges of 1.5 mm tightness was approximately 1.22 times the experimental result. Considering the fact that in the case of a 1.5 mm oversizing tightness the wedges were flat-shaped without any insertion angle, it was extremely difficult to knock into and push further inside the opening, especially in cases of a small opening height, both in practice and in the modeling simulation. Excessive deformation may have already occurred during the knocking and push-in processes, considering the harsh insertion conditions; however, it is almost impossible to measure the deformation during the insertion process in practice. Using the finite element method, excessive distortion of the elements on the upper edges of the wedges could be observed during the insertion process owing to the squeezing and friction between the opening and the oversized wedges, which might lead to greater discrepancies in the initial stress of the wedges and consequently the initial stiffness of the joint. For the other two wedge configurations with certain insertion angles, the racking resistant performance in the elastic stage of FEA results was almost in agreement with the experimental results, suggesting that the finite element method can precisely predict the elastic stage behaviors reflected in the corresponding initial stiffness of joints with wedges, particularly those with certain insertion angle. Although the secondary stiffness after yielding was lower than that in the experimental results, the plastic stage behaviors of the FEA results did not significantly diverge from the experimental results, suggesting that the post-yield finite element method can provide a conservative evaluation of the racking resistance of through joints with inclined wedges. Overall, it was confirmed that the finite element method can accurately make a reasonable and reliable evaluation of the racking resistance of mortise–tenon joints and joints with wedges, especially in the elastic stage, where a considerably precise initial stiffness can be predicted by FEA with proper modeling and setup for simulation.

Table 5. Comparative results initial stiffness

$K_{FEM}/$	TJ	RK	HL	TJ3- Δ 1	TJ3- Δ 1.5	TJ3- Δ 2
$K_{Exp.}$	1.03	1.13	1.05	1.13	1.22	1.09



(a) Comparison with mortise-tenon joints



(b) Comparison with wedge-reinforced through joints

Figure 8. Comparative results of the relationship between rotation angle and moment

6.3 STRESS AND DEFORMATION ANALYSIS

As shown in the red box in Fig. 9, the stress development during the entire numerical simulation process was further examined for elements corresponding to the stress concentration areas of each mortise–tenon joint numerical model. The rotation angle at which the corresponding stress exceeded the reference strength, leading to failure, was identified for the stress concentration areas. Fig. 10–12 show the stress–rotation relationships for the stress concentration areas of each type of mortise–tenon joint. In the through joint model, the compressive stress S33 perpendicular to the grain was symmetrically distributed along the centerline of the beam-length direction. The stress around the edge of the embedding areas was generally not significant. After the rotation angle reached 0.08 rad, a slight progression was observed along the width direction of the Nuki, leading to a rapid increase in stress for elements close to the centerline, which then stabilized towards the element at the centerline of the Nuki. This result suggested that embedment was mainly generated in areas between the ends and center of the Nuki along its interface. Additionally, it was confirmed that the compressive stress S33 along the tangential direction in the crucial contact areas exceeded the reference standard embedment strength (7.8 MPa) at a rotation angle of 0.041 rad (0.061 minus 0.02 rad of clearance), which approximately corresponds to the yield angle (0.046 rad)

observed in the through joint experimental results. The compressive stress distribution S_{33} of the first element at the embedding edge on the top and the following elements located along the height direction of the Nuki indicated that the compressive stress perpendicular to the grain propagated from the embedding areas on the top to the bottom of the Nuki, with a significant reduction in stress in the upper elements along the Nuki height, followed by a gradual decrease, revealing a trend of stress variation in the Nuki height direction. The stress reached nearly zero at approximately $7/8$ of the height from the embedding area to the bottom, confirming that the stress distribution of the through joint model was asymmetrical in the FEA simulation. In the Ryakukama joint model, the development of stress parallel to the grain in the three elements at the corner of the Ryakukama tenon's interlocking jaw was examined, showing that the maximum compressive stress at the tenon edge was approximately 3.7 MPa, which is approximately half the reference value of the shear strength of Japanese cypress (7.5 MPa). This result further confirms the former stress distribution result for the Ryakukama joint, where the shear failure observed in the experimental results at the tenon edge did not primarily occur in the upper middle part of the tenon's interlocking jaw. From the aforementioned stress distribution result, shear failure might occur owing to the high compressive stress concentrated at the top and bottom edges of the tenon's interlocking pair, which was observed to be approximately 7.65 MPa, exceeding the reference shear strength. In the half-lap joint model, the stress-rotation relationship for the three elements at the upper edge of the square plug hole showed that the first element at the corner of the plug hole experienced unexpected significant deformation owing to squeezing and friction when the square plug began to rotate and then interfered with the plug hole, which might be the reason for the large discrepancy in stress development with the other two elements. The stress development trends for the second and third elements were generally consistent, and the stress increased almost linearly with the rotation, exceeding the reference shear strength (7.5 MPa) at a rotation angle of 0.1 rad. Therefore, it is highly possible that shear failure occurred at the corner of the square plug hole when the rotation angle reached 0.1 rad. The FEA results, which showed a reasonably good correlation with the experimental results, revealed the potential of the FEA simulation to predict the moment resistance performance of various mortise-tenon joints by studying the stress distribution and development of elements located at crucial contact areas.

7 – CONCLUSION

This study examined the moment resistance performance of traditional timber structures, focusing on the effects of the column-Nuki joint specifications on the bearing capacity and racking resistance. By comparing the experimental testing and FEA, the following conclusions were drawn:

- 1) The initial stiffness of the Ryakukama and plug-reinforced half-lap joints was significantly higher than that of the through joints, with the Ryakukama joint achieving 1.66 times the stiffness of the through joint. Column-Nuki joints with wedge insertion effectively improved their stiffness, achieving up to 2.8 times the stiffness of through joints without wedges.
- 2) Comparisons of moment-rotation relationships and stress distribution in crucial areas confirmed that with clear definitions of elasticity and plasticity and fine joint deformations, FEA can predict the bearing capacity, rotational deformation, and possible failure of different mortise-tenon joint types with adequate precision.

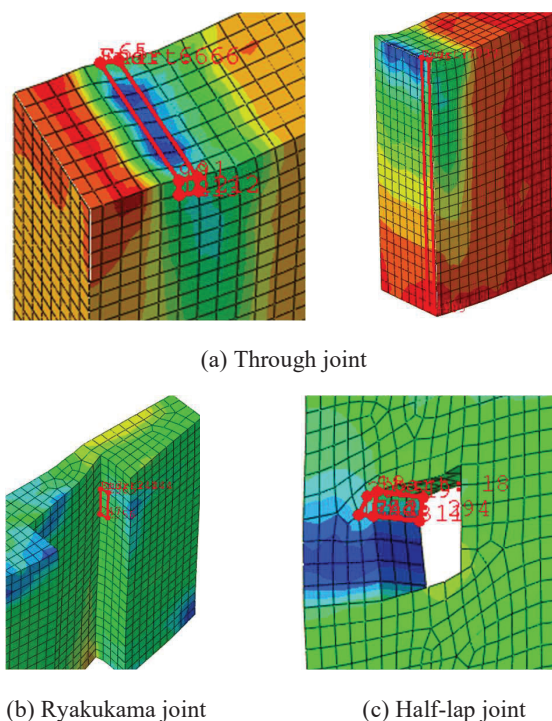
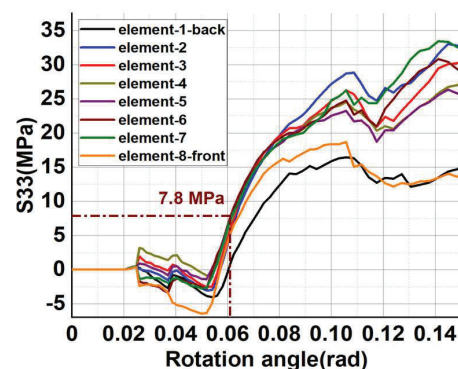
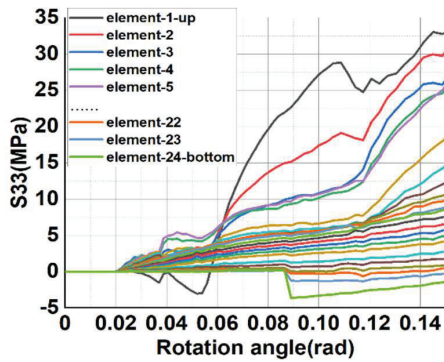


Figure 9. Elements in the stress development analysis



(a) Elements located along the radial direction



(b) Elements located along the tangential direction

Figure 10. Stress–rotation: through joint

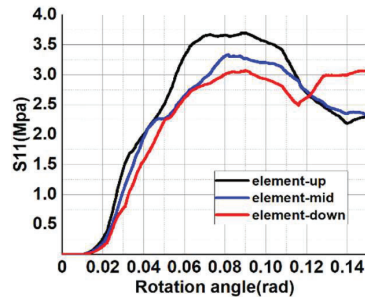


Figure 11. Stress–rotation: Ryakukama joint

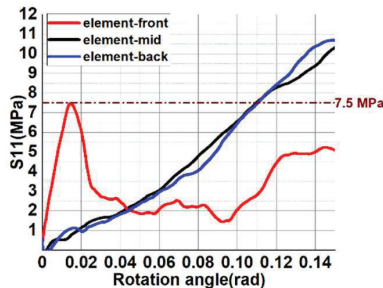


Figure 12. Stress–rotation: half-lap joint

8 – REFERENCES

[1] T. Guo, N. Yang, and H. B. Zhou. “Experimental study of the seismic performance of Chuan-Dou-style longitudinal wooden frame.” In: *China Civil Engineering Journal* 54 (2021), pp. 34–41.

[2] H. B. Xiong, J. Wang, and L. Wu. “Experimental study on lateral resistance performance of Chuandou wooden frame structures.” In: *Journal of Building Structures* 39.10 (2018), pp. 122–129.

[3] B. Wang, G. L. Bai, and C. Q. Wang. “Study on the seismic response and construction measure of the Chuandou wooden structure.” In: *Journal of Xi’an University of Architecture and Technology (Natural Science Edition)* 46.4 (2014), pp. 536–541.

[4] X. W. Wang, B. T. Sun, and H. F. Chen. “Analysis of architectural and structural characteristics and typical

earthquake damage to the Chuandou-type timber frame in Southwest China: A case study of the mountainous areas in Guizhou Province.” In: *Journal of Seismology Research* 47.2 (2024), pp. 290–299.

[5] Z. Qu, A. Dutu, J. R. Zhong, and J. Sun. “Seismic damage to masonry-infilled timber houses in the 2013 M7.0 Lushan, China, earthquake.” In: *Earthquake Spectra* 31.3 (2015), pp. 1859–1874. <https://doi.org/10.1193/012914EQS023T>

[6] M. Inayama. “Study on compression perpendicular to the grain in wood. Part 4: Analytic functions for the relation between compression load and elastic deformation perpendicular to the grain in wood.” In: *Technical Papers of Annual Meeting AIJ* (1993), pp. 907–908.

[7] H. Noguchi, M. Kobayashi, and Y. Hashidume. “Study and suggestion on allowable partial compressive stress perpendicular to grain: Study on compressive stress perpendicular to grain.” In: *Journal of Structural and Construction Engineering AIJ* 518 (1999), pp. 65–70.

[8] A. Kitamori, Y. Kato, Y. Kataoka, and K. Komatsu. “Proposal for a mechanical model of beam-column ‘Nuki’ joints in traditional timber structures.” In: *Mokuzai Gakkai Shi* 49 (2003), pp. 179–186.

[9] W. Liu, B. Chen, and Y. Huang. “Analysis of timber frame based on different nodes in ABAQUS.” In: *China Forest Products Industry* 60.5 (2023), pp. 59–67.

[10] W. S. Chang and M. F. Hsu. “Estimating rotational stiffness of timber joints by using fractional factorial experiments combined with computer simulation.” In: *8th World Conference on Timber Engineering* (2004).

[11] Y. Luo. “Study on the mechanics characteristics and seismic behavior of ancient timber buildings frame assembled with mortise-and-tenon joints.” PhD thesis. Xi’an University of Architecture and Technology, 2006.

[12] Z. Y. Chen. “Behavior of typical joints and the structure of Yingxian Wood Pagoda.” PhD thesis. Harbin Institute of Technology, 2011.

[13] Z. W. Guan, A. Kitamori, and K. Komatsu. “Experimental study and finite element modelling of Japanese ‘Nuki’ joints—Part one: Initial stress states subjected to different wedge configurations.” In: *Engineering Structures* 30.7 (2008), pp. 2032–2040. <https://doi.org/10.1016/j.engstruct.2008.01.003>

[14] A. Aloisio, M. M. Rosso, A. Iqbal, and M. Fragiacommo. “Hysteresis modeling of timber-based structural systems using a combined data and model-driven approach.” In: *Computers & Structures* 269 (2022), <https://doi.org/10.1016/j.compstruc.2022.106830>

[15] Japan Housing & Wood Technology Center. “Allowable stress calculation of house constructed by wooden framework method.” In: (2008), pp. 563–578.

[16] A. Sauda, K. Aoki, and M. Inayama. “Evaluation of bearing capacity on timber grid walls considering clearance of crosspiece joints.” In: *AIJ Journal of Technology and Design* 29.73 (2023), pp. 1302–1307. <https://doi.org/10.3130/aijt.29.1302>

[17] Architectural Institute of Japan. “Design manual for engineered timber joints.” In: (2009).